Arch Appl Mech (2006) 75: 164–176
DOI 10.1007/s00419-005-0427-0

ORIGINAL

C. C. Tsai · C. H. Tseng

The effect of friction reduction in the presence of in-plane vibrations

Received: 12 June 2004 / Accepted: 9 August 2005 / Published online: 9 December 2005

Abstract A reduction of friction by vibrations has been observed in various experiments. This effect can be applied to actively control frictional forces by modulating vibrations. Moreover, common methods of controlling friction rely on lubricants and suitable material combinations. The superimposition of vibrations can further reduce the friction force. This study presents a theoretical approach based on the Dahl friction model that describes the friction reduction observed in the presence of the tangential vibrations at an arbitrary angle. Analysis results indicated that the tangential compliance should be considered in modeling the effect of vibrations in reducing friction. At any vibration angle, the tangential compliance of the contacts reduces the friction reduction effect. The vibrations parallel to the macroscopic velocity are most effective for friction reduction.

Keywords Friction · Vibration · Modeling · Dahl

1 Introduction

A reduction of friction by vibrations has been observed in various experiments. The vibration direction can be either normal [11–14, 16, 23, 24] or tangential [3, 15, 17–20] with respect to the contact surface. This effect can be used for the reduction of process force in manufacturing processes, such as ultrasonic machining and ultrasonic-vibration drawing [9], or solving the problem of position control in high vacuum environments, such as electron microscopes, where friction can be controlled through the variation of the vibration amplitude only.

To explore the origin of ultrasound-induced friction reduction, Hesjedal and Behme [10] experimentally studied the friction reduction phenomena in microscopic mechanical contacts. They concluded that the friction reduction effect results entirely from the vertical oscillation component. However, previous experimental investigations on tangential vibration showed friction reduction [17–20]. Quantitative analytical models based on the rigid Coulomb friction show the same tendency as the experimental data, but these models have lower values. For these types of contacts, with small amplitude of sliding displacement, Tani [22] showed that the rigid Coulomb friction model was insufficient to describe the friction behavior.

On the microscopic level, apparently smooth surfaces are still "rough." The surface topography plays an important role in surface interactions. When these surfaces are pressed against each other, the true contact area usually is from 1/400 to 1/10,000 of the apparent area observed by the naked eye, as shown in Fig. 1. The protuberant features are called asperities. One of the oldest and simplest microcontact models is the Greenwood–Williamson model [7], which assumed that surfaces were composed of hemispherically tipped asperities. The asperities have a uniform sphere radius and a symmetrical Gaussian distribution of asperity

C. C. Tsai (✉) · C. H. Tseng
Department of Mechanical Engineering, National Chiao Tung University Hsinchu 30056, Taiwan, R. O. C
E-mail: chtseng@cc.nctu.edu.tw
Tel.: +886-3-5726111
Fax: +886-3-5717243

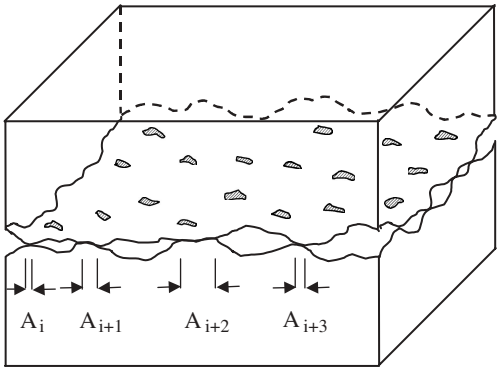

Fig. 1 True contact between surfaces

heights. The Hertz equations governing elastic contact of spheres and half spaces are used to compute the load, contact area, and contact pressure acting on a deformed asperity.

Experiments have observed that when two contacting surfaces slide against each other, a motion of one surface over the other occurs before actual body sliding begins. This effect occurs with the tangential compliance of the asperities. The movement caused by the applied force below the breakaway force is called the presliding displacement or microslip [8,21].

Dahl [4] formulated a mathematical model of the presliding displacement by incorporating tangential compliance. The model acts as a nonlinear spring with a nearly linear elastic response for small deflections, which yields and approaches an asymptotic value for large deflections. Bliman [2] studied the existence and uniqueness of solutions and hysteresis effects of the model.

This study combines the approach proposed by Matunaga and Onoda with the Dahl friction model to analyze the effect of friction reduction by tangential vibrations at any angle.

2 Sliding of rigid body

First, the approach proposed by Matunaga and Onoda is outlined here. The friction system under investigation comprises a rigid body sliding over a rigid and flat plane at a prescribed velocity under constant normal force, as shown in Fig. 2. The prescribed velocity consists of two components. The first component is a macroscopic constant velocity v_b, and the second is a harmonic velocity $(v_v \cos \omega t)$ representing the vibration.

Let θ denote the angle of the harmonic velocity $(v_v \cos \omega t)$ with constant velocity v_b that is parallel to the x-axis. The velocity of the rigid body can be expressed as the vector

$$\vec{v} = (v_b + v_v \cos(\omega t) \cos\theta)\vec{i} + v_v \cos(\omega t) \sin\theta \vec{j} \ . \tag{1}$$

Since the Coulomb friction works on the body in the opposite direction to the relative sliding velocity, the instantaneous Coulomb friction becomes

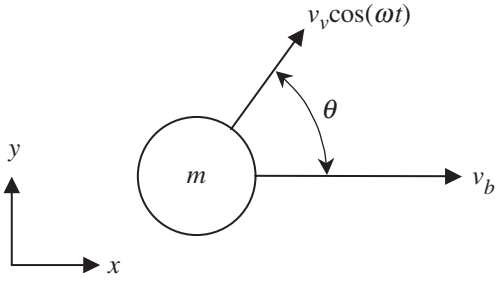

Fig. 2 An analytical model for sliding with tangential vibrations

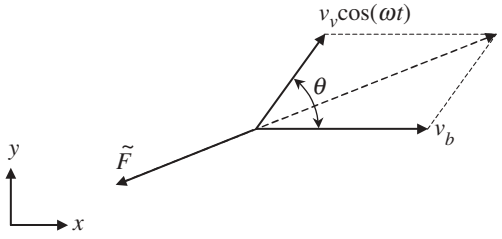

Fig. 3 Friction and velocities

$$\vec{F} = -\mu F_{\mathrm{N}} \frac{\vec{v}}{\left|\vec{v}\right|} = \tilde{F}_x \vec{i} + \tilde{F}_y \vec{j}\,, \tag{2}$$

where F_{N} represents the normal force, as shown in Fig. 3. The components of the friction are given by

$$\tilde{F}_x(\tau) = \frac{-\zeta - \cos\theta\cos\tau}{\sqrt{\zeta^2 + 2\zeta\cos\theta\cos\tau + \cos^2\tau}} \mu F_{\mathrm{N}}, \tag{3}$$

$$\tilde{F}_y(\tau) = \frac{-\sin\theta\cos\tau}{\sqrt{\zeta^2 + 2\zeta\cos\theta\cos\tau + \cos^2\tau}} \mu F_{\mathrm{N}}, \tag{4}$$

where τ is the normalized time defined as

$$\tau = \omega t \tag{5}$$

and ζ denotes the velocity ratio defined as

$$\zeta = \frac{v_b}{v_v}\,. \tag{6}$$

The mechanism of friction reduction by tangential vibrations is illustrated in Fig. 4. The velocity of the sliding body frequently changes its direction in accordance with the vibration component, and the direction of the Coulomb friction also changes. Because the amplitude of the Coulomb friction remains constant, the friction force in the direction of v_b reduces on time-average.

The effective friction force that is observed macroscopically is the time-averaged friction force. The time-averaged friction force in the direction of x (macroscopic velocity v_b) is defined as

$$\bar{F}_x = \frac{1}{2\pi} \int_0^{2\pi} \tilde{F}_x(\tau) d\tau\,. \tag{7}$$

The effect of friction reduction by superposed vibrations can be described quantitatively by the ratio

$$r = \frac{\bar{F}}{F} \tag{8}$$

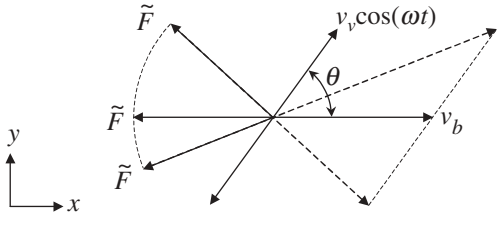

Fig. 4 Mechanism of time-average friction reduction

of the time-averaged friction force $\bar{F}$ to the friction force $F = -\mu F_{\mathrm{N}}$ observed in the absence of vibrations. The friction ratio in the direction of x becomes

$$r_x(\zeta, \theta) = \frac{1}{2\pi} \int_0^{2\pi} \frac{\zeta + \cos\theta \cos\tau}{\sqrt{\zeta^2 + 2\zeta \cos\theta \cos\tau + \cos^2\tau}} d\tau \,. \tag{9}$$

It can be calculated explicitly if $\theta = 0$ and $\theta = \pi/2$ as follows:

$$r_x(\zeta, 0) = \begin{cases} \frac{2}{\pi} \sin^{-1}\zeta, & 0 \le \zeta \le 1, \\ 1, & \zeta > 1\,, \end{cases} \tag{10}$$

$$r_x(\zeta, \frac{\pi}{2}) = \frac{2}{\pi} \frac{\zeta}{\sqrt{1+\zeta^2}} K\left(\frac{1}{1+\zeta^2}\right), \tag{11}$$

where $K(m)$ is the complete elliptic integral of the first kind. The friction ratio r_x for different angles is plotted in Fig. 5. The friction ratio decreases with decreasing velocity ratio ζ. A significant friction reduction effect is observed whenever the macroscopic velocity is smaller than the velocity amplitude of the vibration component. For velocity ratio $\zeta < 0.95$, the vibration parallel to the direction of the macroscopic velocity ($\theta = 0$) exerts the greatest effect on the friction reduction. For velocity ratio $\zeta > 1$, the vibration perpendicular to the direction of the macroscopic velocity ($\theta = \pi/2$) has a larger effect on the friction reduction, but this effect is not significant. It is important to recognize that the superposed vibrations reduce the time-averaged friction force, not the real friction.

3 Sliding with tangential compliance

Surfaces are very irregular at the microscopic level. Therefore, two surfaces contact at a number of asperities. When a tangential force is applied, the asperities will deflect like springs giving rise to the friction force. If the strain of any particular asperity exceeds a certain level, the bond will be broken and a new bond having a smaller strain will be established. Dahl modeled the average stress–strain curve by a differential equation. Let x be the displacement of the sliding body, F the friction force, and F_{c} the Coulomb friction force. Then Dahl's model has the form

$$\frac{dF}{dx} = \sigma_0 \left(1 - \frac{F}{F_c} \mathrm{sgn}(v)\right)^i \,, \tag{12}$$

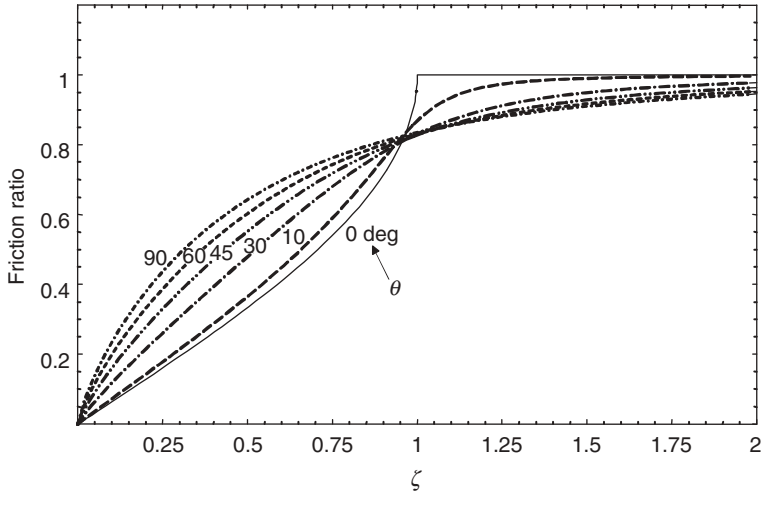

Fig. 5 Friction ratio r_x for different angles

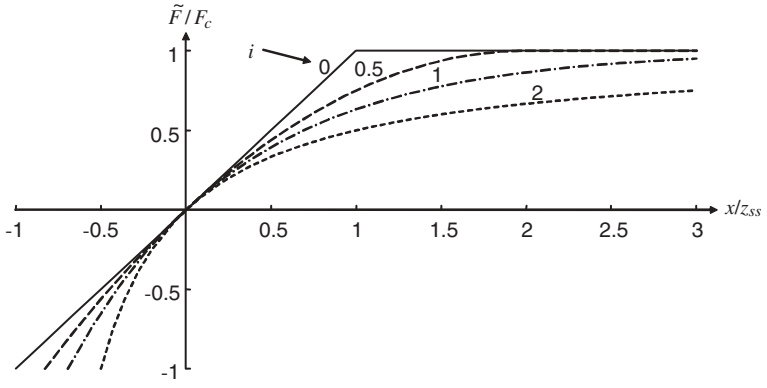

Fig. 6 Friction–displacement curves for $v > 0$

where σ_0 is the contact stiffness or slope of the force–deflection curve at $\tilde{F} = 0$ and i is a parameter that determines the shape of the stress–strain curve, as illustrated in Fig. 6. The average behavior of the asperities can be represented by the physical analogy depicted in Fig. 7. Here, the sliding body experiences a friction force due to the deformation of a single lumped asperity contact. Hence, the friction force can be defined as

$$F = \sigma_0 z\,, \tag{13}$$

where z is the deflection of the lumped asperity that is defined as the horizontal distance between points P and T. Then the Dahl model can be written as

$$\frac{dz}{dt} = v\left(1 - \frac{\sigma_0}{F_c}\mathrm{sgn}(v)z\right)^i\,. \tag{14}$$

Equation (14) claims that during the unidirectional sliding the deflection z approaches the magnitude

$$z_{ss} = \frac{F_c}{\sigma_0}\,, \tag{15}$$

which is the steady-state deflection of the asperity. Thus (14) can be written as

$$\frac{dz}{dt} = v\left(1 - \frac{z}{z_{ss}}\mathrm{sgn}(v)\right)^i\,. \tag{16}$$

The hypothesis of the Dahl model, including most friction models, is that the friction force is parallel to the velocity of the sliding body. Some difficulties arise in modeling the asperity behavior in the friction system as shown in Fig. 2, where the instantaneous friction force may not be parallel to the velocity of the sliding body. In this friction system, the velocity of the sliding body frequently changes direction in accordance with the vibrations. The vibration direction must be parallel to the direction of the macroscopic velocity (i.e., $\theta = 0$) for the instantaneous friction force to be parallel to the velocity of the sliding body, and the Dahl model can then be applied without difficulty. However, the behavior of the lumped asperity becomes more complicated when the direction of vibrations is not parallel to the direction of the macroscopic velocity (i.e., $\theta \neq 0$).

Figure 8 shows the behavior of the lumped asperity when the sliding body moves along a curve. This figure is the top view of Fig. 7, and only points P and T are shown. The trajectory of point P of the sliding body

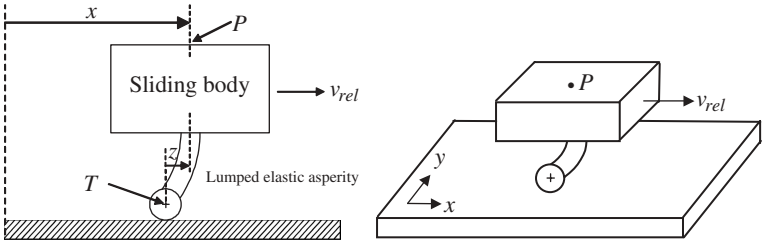

Fig. 7 The friction interface between two surfaces is thought of as a lumped elastic asperity

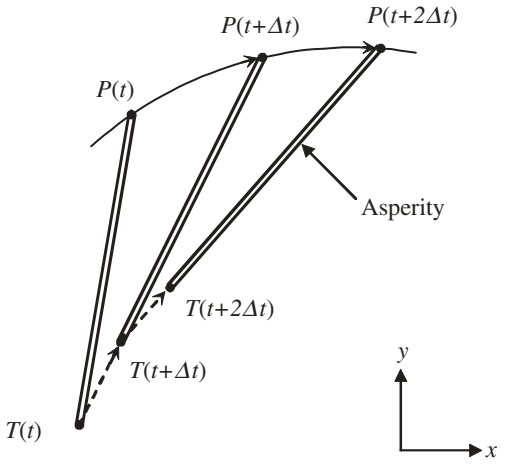

Fig. 8 Behavior of lumped asperity (*top view*)

is known, and the trace of point T of the asperity needs to be determined to calculate the friction force. The trace of point T can be approximated by the following procedure. At time t, point P of the sliding body is in position $P(t)$ and point T of the asperity is in position T(t). At time $(t + \Delta t)$, point P of the sliding body moves to position $P(t + \Delta t)$. If the time increment Δt is small, the asperity is pulled approximately along line $\overline{T(t)P(t + \Delta t)}$ to a new position $T(t + \Delta t)$. The length of line $\overline{T(t + \Delta t)P(t + \Delta t)}$, namely the new deflection of the asperity, depends on the friction force and the elasticity of the asperity, which are discussed below. Following this scheme and using a small time change Δt can obtain the trace of point T, as shown in Fig. 9.

3.1 Asperity slip without a stiction phase (Dahl model with $i = 1$)

Referring to the Dahl model, Eq. (14), the deflection change after a small time increase Δt can be expressed as

$$\Delta z \approx v(t)\left(1 - \frac{\sigma_0}{F_c}\mathrm{sgn}(v(t))z(t)\right)\Delta t\,, \tag{17}$$

where the value $i = 1$ is used. Obviously Δz approaches zero as the deflection $z(t)$ approaches the steady-state deflection ($z_{ss} = \sigma_0/F_c$). The deflection of the asperity at time t is given by

$$z(t) = \overline{T(t)P(t)} = \sqrt{(P_x(t) - T_x(t))^2 + (P_y(t) - T_y(t))^2}\,, \tag{18}$$

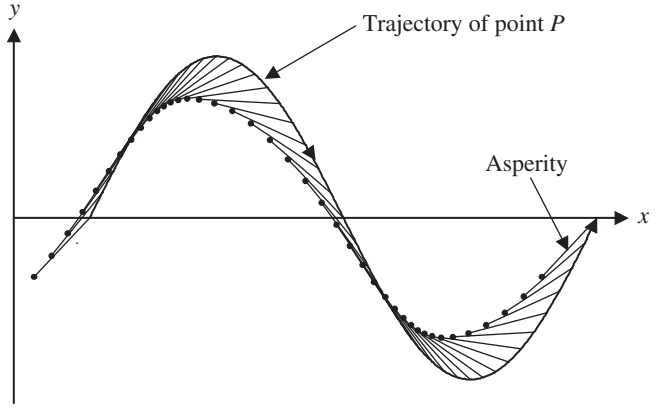

Fig. 9 Behavior of lumped asperity over one steady-state period

where $P(t) = (P_x(t), P_y(t))$ and $T(t) = (T_x(t), T_y(t))$. The velocity $v(t)$ in (17) can be approximated by the mean velocity of point P along line $\overline{T(t)P(t+\Delta t)}$, namely

$$v(t) \approx \frac{\overline{T(t)P(t+\Delta t)} - \overline{T(t)P(t)}}{\Delta t} = \frac{\sqrt{(P_x(t+\Delta t) - T_x(t))^2 + (P_y(t+\Delta t) - T_y(t))^2} - z(t)}{\Delta t} . \tag{19}$$

According to (17), the deflection of the asperity at time $(t + \Delta t)$ is written as

$$z(t+\Delta t) = z(t) + \Delta z \approx z(t) + v(t)\left(1 - \frac{\sigma_0}{F_c}\mathrm{sgn}(v(t))z(t)\right)\Delta t , \tag{20}$$

which can be obtained by inserting (18) and (19). Once the new deflection of the asperity at time $(t + \Delta t)$ is obtained, the new position of point T, $T(t + \Delta t)$, is given by

$$T_x(t+\Delta t) = P_x(t+\Delta t) - \frac{z(t+\Delta t)}{\overline{T(t)P(t+\Delta t)}}(P_x(t+\Delta t) - T_x(t)), \tag{21}$$

$$T_y(t+\Delta t) = P_y(t+\Delta t) - \frac{z(t+\Delta t)}{\overline{T(t)P(t+\Delta t)}}(P_y(t+\Delta t) - T_y(t)). \tag{22}$$

The friction force depends on the deflection and the direction of the asperity. The friction force at time $(t + \Delta t)$ therefore can be expressed as [refer to (13)]

$$F_x(t+\Delta t) = \sigma_0(P_x(t+\Delta t) - T_x(t+\Delta t)) , \tag{23}$$

$$F_y(t+\Delta t) = \sigma_0(P_y(t+\Delta t) - T_y(t+\Delta t)), \tag{24}$$

which is the component form of the friction force. Following (18)–(24), the friction force at time $(t+2\Delta t)$ can be obtained. Continuing this process, we can obtain the friction force during sliding with tangential vibrations.

3.2 Asperity slip with stiction phase (Dahl model with $i = 0$)

Equation (14) shows that in the Dahl model with $i \neq 0$ the asperity can slip [i.e., $dz \neq v(t)dt$], even when the deflection is very small. Thus, when an oscillatory applied force that is far smaller than the Coulomb friction F_c is applied to the sliding body, the position of the sliding body drifts. To minimize this drift, Dupont et al. [5,6] proposed an elastoplastic friction model that possesses a stiction phase. The asperity sticks [i.e., $dz = v(t)dt$] when its deflection is smaller than a breakaway deflection. Consequently, it is reasonable to assume that the asperity as shown in Fig. 8 sticks when its deflection is smaller than the steady-state deflection. Here, the value $i = 0$ is used in the Dahl model to render stiction. The Dahl model then reduces to

$$\frac{dz}{dt} = \begin{cases} v(t) , & z < z_{ss} , \\ 0 , & z \geq z_{ss} , \end{cases} \tag{25}$$

$$F = \sigma_0 z, \tag{26}$$

which is essentially an elastic Coulomb friction model. The asperity is modeled as a linear spring. When an increasing tangential force is applied, the asperity does not slip until the force increases to the size of the Coulomb friction F_c. Before slippage, the deflection of the asperity equals the displacement of the sliding body. Thus, the deflection of the asperity at time $(t + \Delta t)$ in Fig. 8 can be written as

$$z(t+\Delta t) = \begin{cases} \overline{T(t)P(t+\Delta t)}, & \overline{T(t)P(t+\Delta t)} < z_{ss} , \\ z_{ss}, & \overline{T(t)P(t+\Delta t)} \geq z_{ss} . \end{cases} \tag{27}$$

Replacing (20) with (27) and following (18)–(24) can yield the friction force during sliding with tangential vibrations.

4 Friction ratio

In the friction system shown in Fig. 2, the trajectory of point P of the sliding body is given by

$$P_x(t) = \zeta v_v t + \frac{v_v}{\omega} \sin(\omega t) \cos\theta \,, \tag{28}$$

$$P_y(t) = \frac{v_v}{\omega} \sin(\omega t) \sin\theta \,. \tag{29}$$

In the steady state, the time-averaged friction force in the directions of x and y are defined as

$$\bar{F}_x = \frac{\omega}{2\pi} \sum_{k=1}^{n} F_x(t + k\Delta t)\Delta t \,, \tag{30}$$

$$\bar{F}_y = \frac{\omega}{2\pi} \sum_{k=1}^{n} F_y(t + k\Delta t)\Delta t \,, \tag{31}$$

where

$$n = \frac{2\pi}{\omega \Delta t} \,. \tag{32}$$

The effect of friction reduction by superposed vibrations can be described quantitatively by the friction ratio in the direction of x, i.e., the direction of the macroscopic velocity, which is given by

$$r_x = \frac{\bar{F}_x}{F_c} = \frac{\omega}{2\pi F_c} \sum_{k=1}^{n} F_x(t + k\Delta t)\Delta t \,. \tag{33}$$

As stated, in the Dahl model the friction force is only a function of the displacement and the sign of the velocity. For the values $i = 1$ or $i = 0$, this property leads to the relation in which the time-averaged friction force is a function of the displacement ratio

$$r_{disp} = \frac{v_v \sigma_0}{\omega F_c} = \frac{v_v/\omega}{F_c/\sigma_0} = \frac{x_v}{z_{ss}} \,, \tag{34}$$

which is a ratio of the displacement amplitude of the vibration component to the steady-state deflection of the asperity. The displacement ratio can be seen as an index of the influence of the tangential compliance on the friction reduction.

Equations (18)–(24) can yield the friction force over one steady-state period. The friction ratios r_x with the value $i = 1$ (without a stiction phase) and $i = 0$ (with a stiction phase) for $\theta = \pi/2$ (perpendicular vibrations) are plotted in Figs. 10 and 11, respectively. The friction ratios for $\theta = 0$ (parallel vibrations) are plotted in Figs. 12 and 13. These figures show that a larger displacement ratio leads to a lower friction ratio. With increasing displacement ratio, the friction ratio approaches that based on the rigid Coulomb friction mode (Fig. 5). Comparing the curve for $i = 1$ with that for $i = 0$ clearly shows that for larger velocity ratios the friction ratios are equal, while for smaller velocity ratios the former drops faster than the latter with decreasing velocity ratio. This result can be explained by the asperity behaviors.

As the velocity ratio ζ decreases, the trajectory of point P of the sliding body is squeezed in the x-axis direction, as shown in Fig. 14. When the sliding body travels along the trajectory with large curvature, the asperity may relax due to the decrease in the horizontal distance between points P and T. Equation (14) shows that during asperity relaxation and stretching, the Dahl model with $i = 1$ has a larger relaxing rate [where $\mathrm{sgn}(v) = -1$] and a lower stretching rate [where $\mathrm{sgn}(v) = 1$] than the Dahl model with $i = 0$, for which $dz/dt = v(t)$. Consequently, over one steady-state period, the friction magnitude of the Dahl model with $i = 1$ is lower that that of the Dahl model with $i = 0$, leading to a lower friction ratio (Figs. 15 and 16).

As the velocity ratio ζ increases, the trajectory of point P of the sliding body is lengthened in the direction of the x-axis, as shown in Fig. 17. If the velocity ratio is sufficiently large, the curvature of the trajectory of point P will be too small to cause a relaxation of asperity. In the steady state, the deflection of the asperity

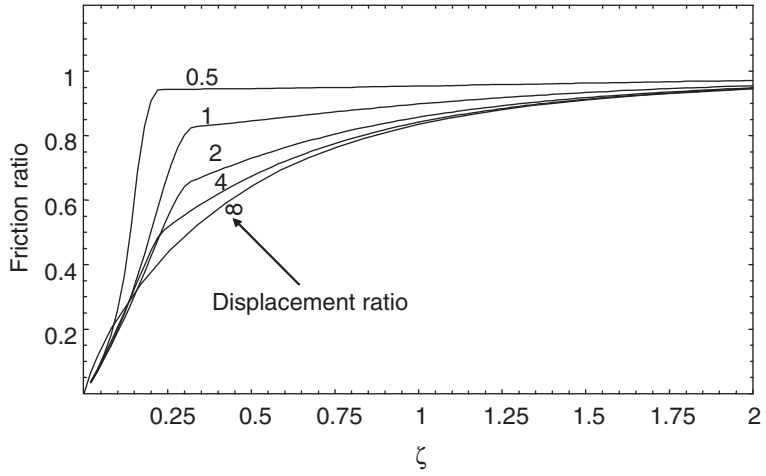

Fig. 10 Friction ratio with $i = 1; \theta = \pi/2$

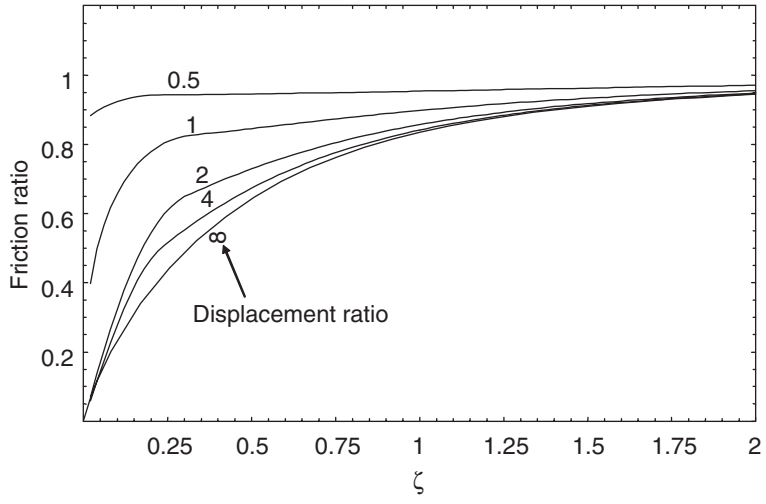

Fig. 11 Friction ratio with $i = 0; \theta = \pi/2$

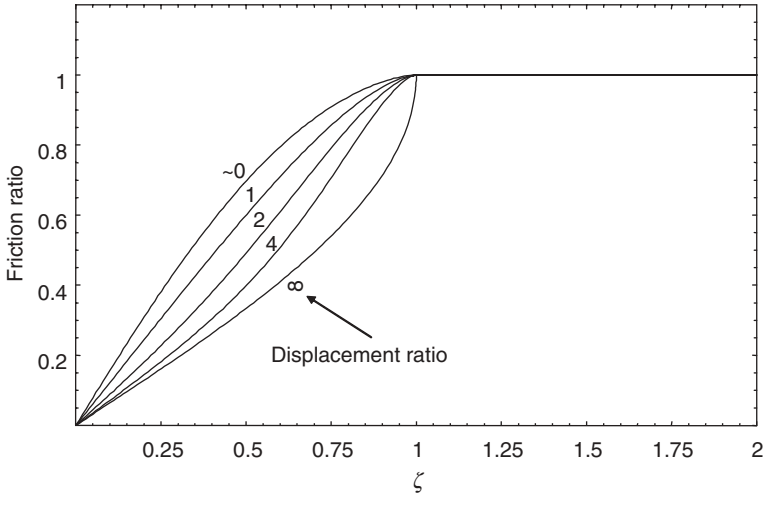

Fig. 12 Friction ratio with $i = 1; \theta = 0$

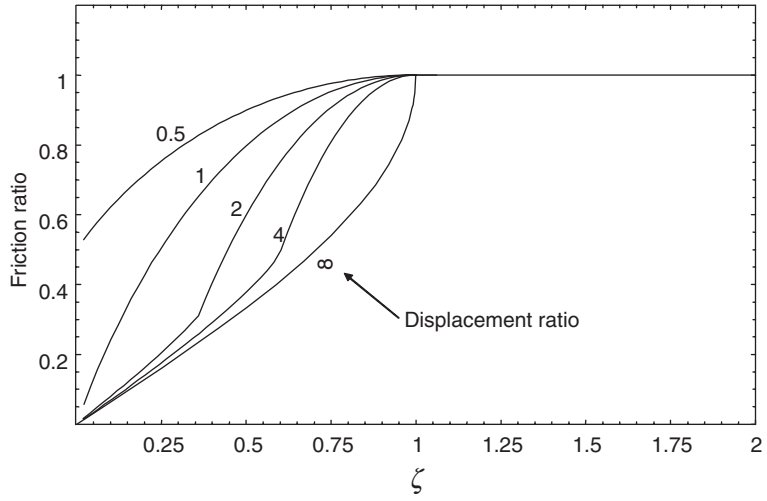

Fig. 13 Friction ratio with $i = 0; \theta = 0$

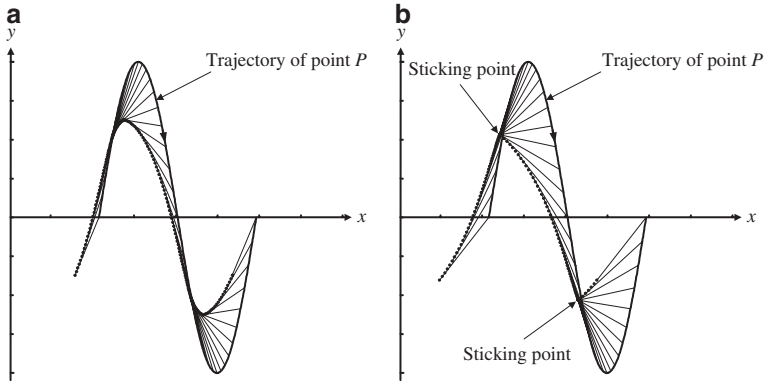

Fig. 14 Comparison of asperity behaviors over one steady-state period ($r_{\text{disp}} = 2, \zeta = 0.15, \theta = \pi/2$). **a** Dahl model without stiction phase ($i = 1$). **b** Dahl model with stiction phase ($i = 0$)

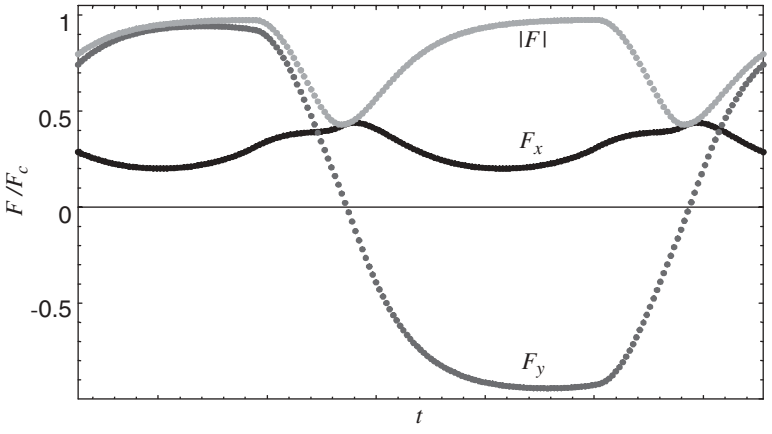

Fig. 15 Friction force over one steady-state period for Fig. 14 (**a**)

reaches the steady-state deflection z_{ss}, namely the magnitude of the friction force remains constant (F_{c}), as shown in Fig. 18. Hence, the Dahl model predicts the same friction ratio in this condition whether $i = 1$ or $i = 0$.

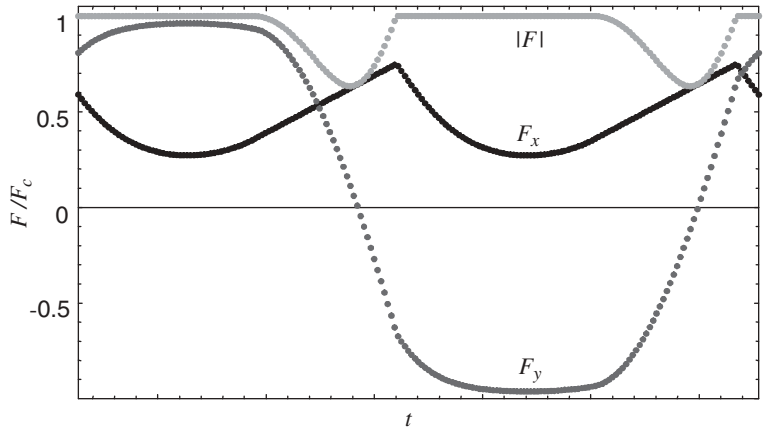

Fig. 16 Friction force over one steady-state period for Fig. 14 (**b**)

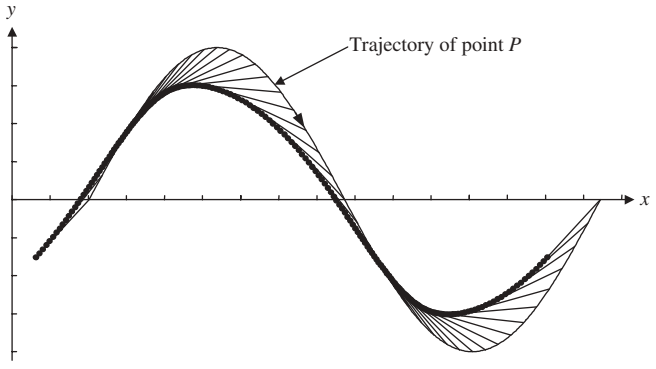

Fig. 17 Behavior of asperity over one steady-state period ($r_{\text{disp}} = 2, \zeta = 0.5, \theta = \pi/2$)

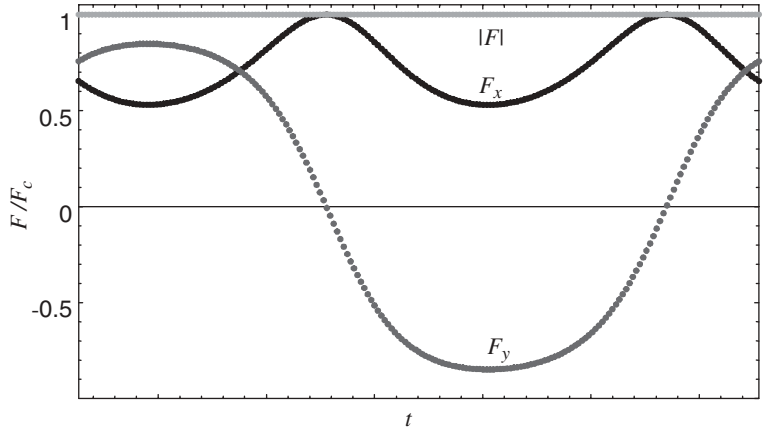

Fig. 18 Friction force over one steady-state period for Fig. 17

Figure 19 shows the comparison of friction ratio between calculated values and experimental results by Littmann et al. The results based on the Dahl model clearly display better agreement with the experimental results than those based on the rigid Coulomb friction model. Additionally, for lower velocity ratios, the results based on the Dahl model with a stiction phase exhibit closer agreement with the experimental results than those without a stiction phase.

One important characteristic of sliding with vibrations is that the superposed vibrations may periodically change the relative sliding direction, and the displacement amplitude of the harmonic component is generally some micrometers (for example displacement amplitude of 0.7 μm at 60 kHz in the experiment by Littmann

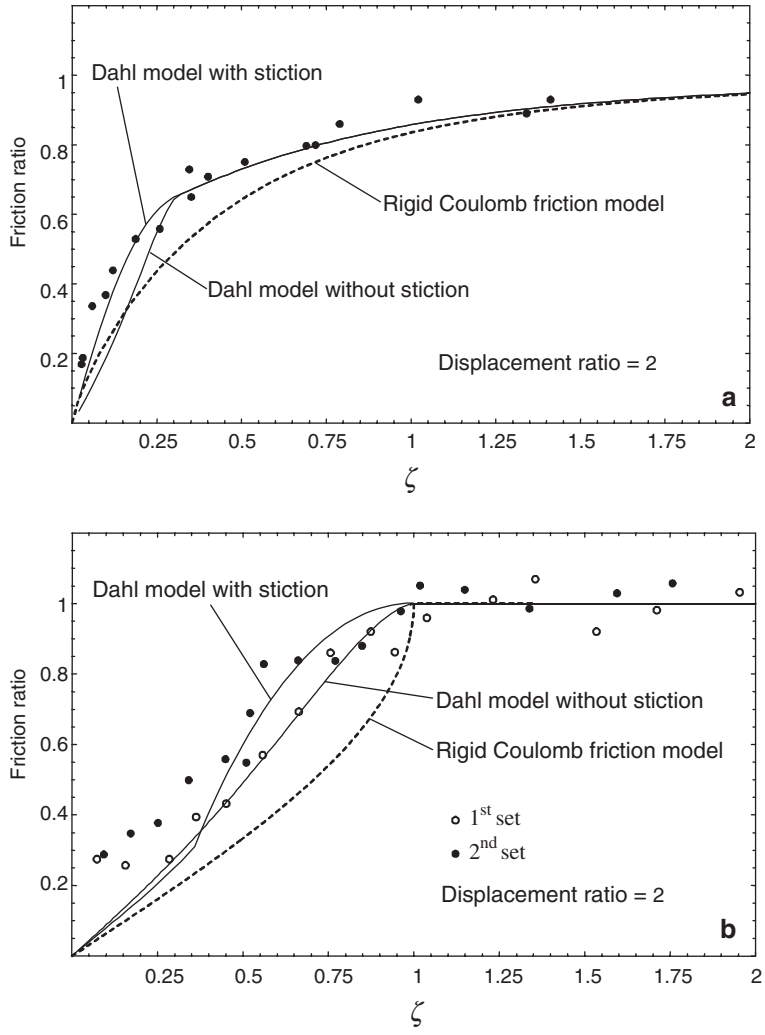

Fig. 19 Comparison of friction ratio between calculated values and experimental results (*dot* and *circle*) by Littmann et al. [18, 19]. **a** Perpendicular vibrations, $\theta = \pi/2$. **b** Parallel vibrations, $\theta = 0$

et al. [17–19]), which is in the same order as the presliding displacement (the presliding displacements of the metals measured in the experiments [1,8,21] are about 0.3–10 μm, which is close to the typical asperity dimension of the finished hard metals). Hence the tangential compliance should be considered in modeling the effect of friction reduction by vibrations. Although the tangential compliance of the Dahl model results from the small-scale asperities, the tangential compliance of the bulk material exerts a similar influence on the friction reduction.

5 Conclusions

This study presents a theoretical approach based on the Dahl friction model that describes the friction reduction observed in the presence of tangential vibrations at an arbitrary angle. The analysis results demonstrate that the vibrations parallel to the macroscopic velocity most effectively reduce the friction. The friction reduction effect is significant whenever the magnitude of macroscopic velocity is smaller than the velocity amplitude of vibration. However, when the magnitude of macroscopic velocity is larger than the velocity amplitude of vibration, the vibrations perpendicular to the macroscopic velocity still take effect and are most effective but the friction reduction is not significant. At any vibration angle, the tangential compliance of the contacts reduces the friction reduction effect. The results obtained using the proposed approach exhibit better agreement with the experimental data than those based on the rigid Coulomb friction model.

Acknowledgements The research reported in this paper is supported under a project sponsored by the National Science Council Grand, Taiwan, R.O.C., NSC91-2212-E-009-022.

References

1. Armstrong, B.: Control of machines with friction. Kluwer, Boston, pp 78–80 (1991)
2. Bliman, P.-A.J.: Mathematical study of the Dahl's friction model. Eur J Mech A Solids **11**, 835–848 (1992)
3. Broniec, Z., Lenkiewicz, W.: Static friction processes under dynamic loads and vibration. Wear **80**, 261–271 (1982)
4. Dahl, P.R.: Solid Friction damping of mechanical vibrations. AIAA J **14**, 1675–1682 (1976)
5. Dupont, P., Armstrong, B., Hayward, V.: Elasto-plastic friction model: contact compliance and stiction. Proc Am Control Conf **2**, 1072–1077 (2000)
6. Dupont, P., Hayward, V., Armstrong, B., Altpeter, F.: Single state elasto-plastic friction models. IEEE Trans Autom Control **47**, 787–792 (2002)
7. Greenwood, J.A., Williamson, J.B.P.: Contact of nominally flat surfaces. Proc R Soc Lond A **295**, 300–319 (1966)
8. Hagman, L.A., Olofsson, U.: Model for micro-slip between flat surfaces based on deformation of ellipsoidal elastic asperities–parametric study and experimental investigation. Tribol Int **31**, 209–217 (1998)
9. Hayashi, M., Jin, M., Thipprakmas, S., Murakawa, M., Hung, J.C., Tsai, Y.C., Hung, C.H.: Simulation of ultrasonic-vibration drawing using the finite element method (FEM). J Mater Process Technol **140**, 30–35 (2003)
10. Hesjedal, T., Behme, G.: The origin of ultrasound-induced friction reduction in microscopic mechanical contacts. IEEE Trans Ultrason Ferroelectr Freq Control **49**, 356–364 (2002)
11. Hess, D.P., Soom, A.: Normal vibrations and friction under harmonic loads: part 1. Hertzian contacts. Trans ASME J Tribol **113**, 80–86 (1991)
12. Hess, D.P., Soom, A.: Normal vibrations and friction under harmonic loads: part 2. Rough planar contacts. Trans ASME J Tribol **113**, 87–92 (1991)
13. Hess, D.P., Soom, A., Kim, C.H.: Normal vibrations and friction at a Hertzian contact under random excitation: theory and experiments. J Sound Vib **153**, 491–508 (1992)
14. Hess, D.P., Soom, A.: Normal vibrations and friction at a Hertzian contact under random excitation: perturbation solution. J Sound Vib **164**, 317–326 (1993)
15. Kuribayashi, K., Shimizu, S., Yuasa, K., Taniguchi, T., Ikeda, Y.: Friction force reduction of conduit guided wire by vibration. In: Proceedings of the international symposium on micro machine and human science, pp 185–189 (1994)
16. Lehtovaara, A.: Influence of vibration on the kinetic friction between plastics and ice. Wear **115**, 131–138 (1987)
17. Littmann, W., Storck, H., Wallaschek, J.: Reduction of friction using piezoelectrically excited ultrasonic vibrations. Proc SPIE Int Soc Opt Eng **4331**, 302–311 (2001)
18. Littmann, W., Storck, H., Wallaschek, J.: Sliding friction in the presence of ultrasonic oscillations: superposition of longitudinal oscillations. Arch Appl Mech **71**, 549–554 (2001)
19. Littmann, W., Wallaschek, J., Mracek, M., Storck, H.: The effect of friction reduction in presence of ultrasonic vibrations and its relevance to travelling wave ultrasonic motors. Ultrasonics **40**, 379–383 (2002)
20. Matunaga, S., Onoda, J.: A novel method of friction force reduction by vibration and its application to gravity compensation. In: Proceedings of the AIAA/ASME/ASCE/AHS/ASC structures, structural dynamics, and materials conference, pp 1531–1537 (1993)
21. Olofsson, U.: Cyclic micro-slip under unlubricated conditions. Tribol Int **28**, 207–217 (1995)
22. Tani, K.: Friction models for a mobile machine using piezo vibration. Int Workshop Adv Motion Control AMC **2**, 717–722 (1996)
23. Tolstoi, D.M., Borisova, G.A., Grigorova, S.R.: Friction reduction by perpendicular oscillation. Sov Phys Dokl **17**, 907–909 (1973)
24. Tworzydlo, W.W., Becker, E.: Influence of forced vibrations on the static coefficient of friction – numerical modeling. Wear **143**, 175–196 (1991)